

# Sensor Location for Effective Fault Diagnosis in Micro Chemical Processes

Osamu Tonomura\*. Satoshi Nagahara. Jun-ichi Kano.  
Manabu Kano. Shinji Hasebe

Department of Chemical Engineering, Kyoto University,  
Kyoto, Japan, (\*e-mail: tonomura@cheme.kyoto-u.ac.jp).

---

**Abstract:** It is clear from worldwide research that micro chemical processes (MCPs) offer a unique approach to the spatial and temporal control of chemical reactions. The well-known advantages of MCPs are often counterbalanced by serious faults such as channel blockage and catalyst deterioration. To realize stable long-term operation of MCPs, it is necessary to develop a monitoring system that can detect and diagnose these faults. In this work, a physical model-based process monitoring system for a tubular microreactor is developed. A state space model is derived by using the orthogonal collocation method, and the extended Kalman filter is used as an observer. The optimal sensor locations are determined so that unknown parameters such as catalyst effectiveness can be estimated most accurately. In addition, the validity of the conventional observability measures in solving the sensor location problems of MCPs is assessed.

*Keywords:* Microreactor, Sensor location, Process monitoring, Parameter estimation, Fault diagnosis.

---

## 1. INTRODUCTION

In microspaces, viscous force, surface tension, conduction heat transfer, and molecular diffusion become dominant. In addition, the contact time and interfacial area between fluids are precisely controlled. These features achievable in microspaces enable us to handle highly exothermic and rapid reactions and to produce fine particles with narrow size distribution (Hessel et al., 2005). However, the above features are often counterbalanced by serious faults such as channel blockage and catalyst deterioration. To realize stable long-term operation of micro chemical processes (MCPs), it is necessary to develop a monitoring and control system suitable for MCPs. Such a system is usually based on the measurements available from installed sensors. However, the existing miniaturized sensors are too expensive in terms of the initial as well as the maintenance costs. In addition, the sensors connected to microreactors in series are not allowed to observe the internal states of microreactors, because they generate dead volume and affect the flow conditions. Therefore, it is important to develop a monitoring system that can estimate unmeasured variables and unknown parameters from a few indirect on-line measurements and quickly detect and diagnose faults. Thus, our technical imperatives are to develop MCPs-oriented sensing devices, to develop a system that can estimate the internal states of MCPs, to propose an approach for effective fault detection and diagnosis in MCPs, etc. So far, there are only few papers about fault detection and diagnosis of MCPs (Kano et al., 2007). In this work, optimal sensor locations for effective fault diagnosis of a tubular microreactor (TMR) are investigated. In addition, the validity of the conventional observability measures in solving the sensor location problems of the TMR is assessed. Finally,

operation policies and control structures for MCPs with an external numbering-up structure are investigated. Two types of operation policies, total flow control and pressure drop control, are compared from the viewpoint of flow uniformity when blockage occurs.

## 2. TUBULAR MICROREACTOR (TMR)

Applications of TMRs can be found in nitration of aromatic compounds, radical polymerization reactions, etc.

### 2.1 Concept of Fault Detection and Diagnosis

The following method to detect and diagnose faults in TMRs is proposed. A limited number of temperature sensors are embedded in walls of TMRs. Wall temperatures are used to estimate unknown parameters such as catalyst effectiveness. At the same time, the optimal sensor location problems have to be solved so that unknown parameters can be estimated most accurately. Previous similar researches on conventional reactors often neglect heat conduction inside walls when constructing their process models. In case of TMRs, it is crucial to rigorously model the wall heat conduction due to high volume ratio of walls to channels. In addition, there are two methods to formulate process models: empirical model-based method and physical model-based method. In this work, the latter method is adopted.

### 2.2 Physical Model

Figure 1 shows a schematic diagram of a TMR. Premixed reactants, A and B, are fed into the inner tube, and a coolant is fed into the outer tube. Each flow is assumed to be plug

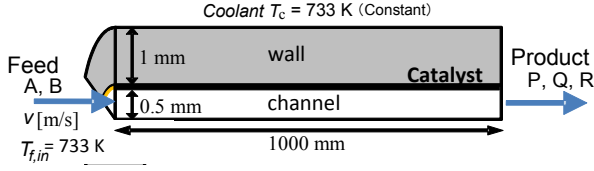


Fig. 1. Schematic diagram of TMR.

flow, and the inner wall surface is coated with a catalyst. On the catalyst surface, the following exothermic reactions take place:



P is a desired product, and Q and R are by-products. The temperature-dependent rate constant  $k_i$  in each reaction is presented by Arrhenius form:

$$k_i = A_i \exp(-E_i/RT_S) \quad , \quad i = 1, 2, 3 \quad (4)$$

Table 1 shows the reaction parameters. A and P are treated as key components, and the TMR can be described by the following mass and energy balance equations:

$$\frac{\partial C_i}{\partial t} = -v \frac{\partial C_i}{\partial z} + D \frac{\partial^2 C_i}{\partial z^2} + D \frac{\partial^2 C_i}{\partial r^2} + D \left( \frac{1}{r} \right) \frac{\partial C_i}{\partial r} \quad (5)$$

$$\frac{\partial T_f}{\partial t} = -v \frac{\partial T_f}{\partial z} + \frac{k_f}{\rho_f C_{pf}} \frac{\partial^2 T_f}{\partial z^2} + \frac{k_f}{\rho_f C_{pf}} \frac{\partial^2 T_f}{\partial r^2} + \frac{k_f}{\rho_f C_{pf}} \left( \frac{1}{r} \right) \frac{\partial T_f}{\partial r} \quad (6)$$

$$\frac{\partial C_{AS}}{\partial t} = -v \frac{\partial C_{AS}}{\partial z} + D \frac{\partial^2 C_{AS}}{\partial z^2} - \frac{k_c}{\delta} \left( C_{AS} - C_A \Big|_{r=d/2} \right) - k_1 C_{AS} - k_2 C_{AS} \quad (7)$$

$$\frac{\partial C_{PS}}{\partial t} = -v \frac{\partial C_{PS}}{\partial z} + D \frac{\partial^2 C_{PS}}{\partial z^2} - \frac{k_c}{\delta} \left( C_{PS} - C_P \Big|_{r=d/2} \right) + k_1 C_{AS} - k_3 C_{PS} \quad (8)$$

$$\frac{\partial T_S}{\partial t} = -v \frac{\partial T_S}{\partial z} + \frac{k_f}{\rho_w C_{pw}} \frac{\partial^2 T_S}{\partial z^2} - \frac{U}{\delta} \left( T_S - T_f \Big|_{r=d/2} \right) - \frac{U}{\delta} \left( T_S - T_w \Big|_{r=d/2} \right) \quad (9)$$

$$\frac{\partial T_w}{\partial t} = \frac{k_w}{\rho_w C_{pw}} \frac{\partial^2 T_w}{\partial z^2} + \frac{k_w}{\rho_w C_{pw}} \frac{\partial^2 T_w}{\partial r^2} + \frac{k_w}{\rho_w C_{pw}} \left( \frac{1}{r} \right) \frac{\partial T_w}{\partial r} - (\Delta H_1 k_1 C_{AS} + \Delta H_2 k_2 C_{AS} + \Delta H_3 k_3 C_{PS}) / (\rho_f C_{pf}) \quad (10)$$

where  $z$  and  $r$  are the axial and radial space coordinates [m], and other variables are summarized in Table 2. Subscripts s, f, and w are catalyst surface, fluid, and wall, respectively. Catalyst thickness,  $\delta$ , is set to 0.2 mm.

### 3 PROCESS MODEL FORMULATION

TMR's physical model described in the previous section is regarded as a real process. Fault diagnosis will be based on a state space model, which is derived from the distributed parameter model (5)-(10).

#### 3.1 Process Model

Using the orthogonal collocation method, each state variable is approximated by the following:

Table 1. Reaction parameters.

Reaction	$A_i$ [1/s]	$E_i$ [J/mol]	$\Delta H_i$ [kJ/mol]
(1)	86760	71711.7	- 2980
(2)	37260	71711.7	- 4622
(3)	149.4	36026.3	- 1664

Table 2. Model parameters.

Parameter	Value	
Reactant velocity $v$	1	m/s
Mass diffusion coefficient $D$	$1 \times 10^{-5}$	$m^2/s$
Heat diffusion coefficient $k_f$	0.041	J/m K s
Heat conductivity of wall $k_w$	16.3	J/m K s
Density of reactant $\rho_f$	1.01	$kg/m^3$
Density of wall $\rho_w$	8000	$kg/m^3$
Viscosity of fluid $\mu$	$2.92 \times 10^{-5}$	Pa s
Heat capacity of reactant $C_{pf}$	1090	J/kg K
Heat capacity of wall $C_{pw}$	500	J/kg K
Reactor length $L$	1	m
Channel diameter $d$	1	mm
Wall thickness $d_w$	1	mm
Inlet conc. of species A $C_A$	4	$mol/m^3$
Inlet conc. of species P $C_P$	0	$mol/m^3$
Inlet temp. of reactant $T_{f,in}$	733	K
Coolant temp. $T_c$	733	K

$$X(t, z, r) \approx \sum_{i=1}^n \sum_{j=1}^m L_i(z) L_j(r) X_{i,j}(t), \quad X = C_A, C_P, T_f, T_w \quad (11)$$

$$X(t, z, r) \approx \sum_{i=1}^n L_i(z) X_i(t), \quad X = C_{AS}, C_{PS}, T_S \quad (12)$$

where  $X_{i,j}(t)$  and  $X_i(t)$  are the value of  $X(t, z, r)$  at the axial collocation points  $z_1 \sim z_n$  ( $0 = z_1 < z_2 < \dots < z_n = L$ ) and the radial collocation points  $r_1 \sim r_m$  ( $0 = r_1 < r_2 < \dots < r_m = d/2$ ), respectively.  $L_i(z)$  and  $L_j(r)$  are Lagrange polynomials. In this study,  $n$  and  $m$  are set to 30 and 5, respectively, and the collocation points are chosen as roots of a Chebyshev polynomial. The above approximation is also applied to the states at boundaries. Equations (5)-(10) are transformed into the following:

$$\dot{\mathbf{x}}(t) = \mathbf{f}(\mathbf{x}(t), \mathbf{u}_{in}) \quad (13)$$

where  $\mathbf{u}_{in}$  denotes the input vector and  $\mathbf{x}$  the state vector:

$$\mathbf{x} = [ C_A^T \quad C_P^T \quad C_{AS}^T \quad C_{PS}^T \quad T_f^T \quad T_S^T \quad T_w^T ]^T. \quad (14)$$

#### 3.2 Observer Design

Nonlinear estimation problems in this research are solved with the extended Kalman filter (EKF), which is based upon the principle of linearization of the state transition matrix and the observation matrix with Taylor series expansions. Wall temperature measurements are used as observed variables. To obtain the best estimates, the locations of the available

sensors must be selected carefully. The sensor location candidates in the axial direction of TMR are prepared according to the collocation points, and the optimal sensor locations are selected according to the following performance index,

$$J = 1 / \left\{ \frac{1}{N} \sum_{k=1}^N \|\theta_{real} - \theta_{est}(k)\|^2 \right\} \quad (15)$$

where  $N$  is the number of iteration steps,  $\theta_{real}$  and  $\theta_{est}$  the real and estimated values of parameters.  $J$  means the rate of convergence towards real values. As  $J$  becomes larger, the estimation performance becomes higher.

#### 4. SIMULATION RESULTS

Three different examples of fault diagnosis of TMR are presented in this section. In addition, the conventional observability measures are examined for the selection of optimal sensor locations in TMR.

##### 4.1 CASE 1: Catalyst Deterioration

In CASE 1, an optimal sensor location problem for estimation of catalyst effectiveness  $\alpha$  is investigated. It is assumed that reaction rate constant  $k_1$  includes  $\alpha$ :

$$k_1(t, z) = \alpha A_1 \exp(-E_1/RT_S(t, z)) \quad (16)$$

An initial value of  $\alpha = 1$  is considered, followed by an abrupt change from 1 to 0.8 at time  $t = t_s$ . After catalyst deterioration,  $\alpha$  is estimated from one temperature measurement by using EKF. The normal steady state ( $\alpha = 1$ ) is used as the initial state of parameter estimation.  $J$  is calculated at every candidate for sensor locations. As shown in Fig. 2 (left), the largest value of  $J$  can be found near the inlet of TMR. This result is well illustrated by Fig. 2 (right). The solid and dotted curves in Fig. 2 (right) correspond to the wall temperature profiles along TMR having  $\alpha = 1$  and 0.8, respectively. The great differences between the solid and dotted curves mean the high responses of temperature to a parameter change. This physical interpretation confirms that the optimal sensor location is near the inlet of TMR.

##### 4.2 CASE 2: Channel Blockage

In CASE 2, a blockage diagnosis problem in TMR is investigated. Specifically, the inlet flow rate is constant, and one temperature sensor is used to estimate fluid velocity  $v$ . An initial value of  $v = 1$  m/s is considered, followed by an abrupt change from 1 m/s to 1.2 m/s at time  $t = t_s$ . After channel blockage,  $v$  is estimated by using EKF. The normal steady state ( $v = 1$  m/s) is used as the initial state of parameter estimation.  $J$  is plotted as a function of sensor position. The relative large values of  $J$  can be found in the latter part of TMR, as seen in Fig. 3 (left). This result is well illustrated by Fig. 3 (right). As well as CASE 1, the large differences between both profiles mean the high responses of temperature to a fluid velocity change. All things considered,

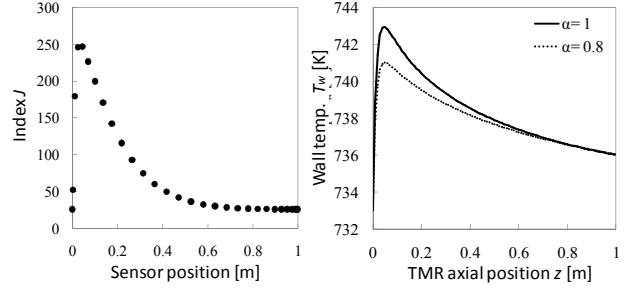


Fig. 2. Estimation results of CASE 1.

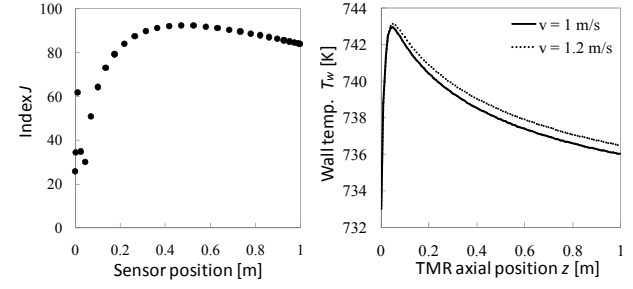


Fig. 3. Estimation results of CASE 2.

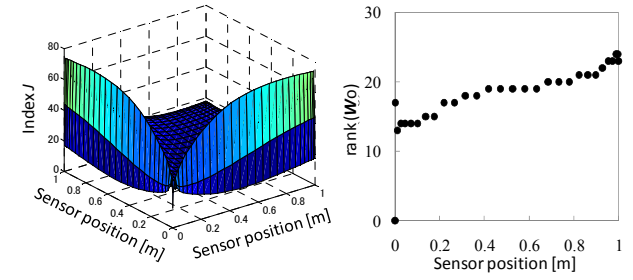


Fig. 4. Results of CASE 3.

Fig. 5. Rank of  $W_o$ .

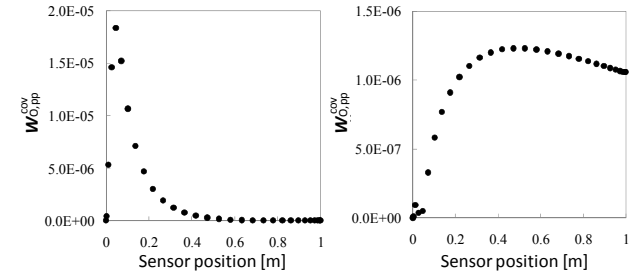


Fig. 6.  $W_{O,pp}^{cov}$  of CASE 1.

Fig. 7.  $W_{O,pp}^{cov}$  of CASE 2.

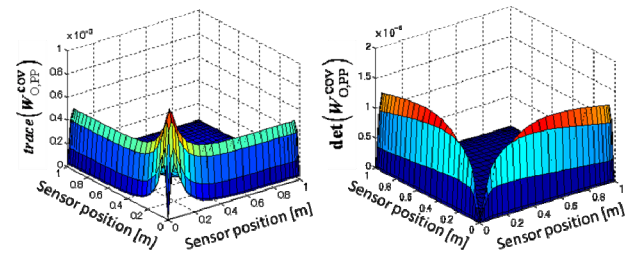


Fig. 8.  $W_{O,pp}^{cov}$  of CASE 3.

Fig. 9.  $W_{O,pp}^{cov}$  of CASE 3.

the optimal sensor location is in the latter part of TMR, which differs from CASE 1.

#### 4.3 CASE 3: Simultaneous Diagnosis of Multi-Faults

This study is similar to the previous cases, but the two unknown parameters,  $\alpha$  and  $\nu$ , are simultaneously estimated by using two temperature sensors. The simulation conditions of the observer are the same as used in the previous cases. Figure 4 suggests that one sensor should be located near the inlet of TMR and the other in the latter part of TMR to realize successful fault diagnosis.

#### 4.4 Observability Measures

Over the years, several studies on sensor locations for estimation in conventional processes have been reported. The representative approaches are to define optimal criteria based on the observability Gramian  $W_O$ . An overview of several criteria is summarized below. Muller et al. (1972) examine the smallest singular value, the determinant, and the trace of  $W_O$  as a measure for sensor location. Dochain et al. (1997) present the condition number of  $W_O$ , and van den Berg et al. (2000) use the trace of  $W_O$  as a criterion for sensor location. While the above presented  $W_O$  is suitable only for linear systems, one alternative is to use the observability covariance matrix  $W_O^{\text{cov}}$  if systems are nonlinear. Singh et al. (2005) present the trace of  $W_O^{\text{cov}}$  for sensor location. The aim of this section is to assess the effectiveness of the existent sensor location criteria for parameter estimation problems in TMR.

In the above presented TMR, observability analysis is performed by determining the rank of  $W_O$ . Figure 5 shows the rank of  $W_O$  at every possible sensor location. Since  $W_O$  at every location is rank deficient, then the system is not observable. In such a situation, the smallest singular value of  $W_O$  is zero. Accordingly, it is not suitable to use criteria such as the smallest singular value, the smallest eigenvalue, the determinant, and the condition number of  $W_O$ . Therefore, the trace of  $W_O^{\text{cov}}$  is appropriate to the determination of the optimal sensor location for parameter estimation. However, for this work,  $W_O^{\text{cov}}$  is used instead of  $W_O$  because the process is a time-variant system in case of parameter estimation problem.  $W_O^{\text{cov}}$  can be decomposed into (Singh et al., 2005):

$$W_O^{\text{cov}} = \begin{bmatrix} W_{O,nn}^{\text{cov}} & W_{O,pn}^{\text{cov}} \\ W_{O,np}^{\text{cov}} & W_{O,pp}^{\text{cov}} \end{bmatrix} \quad (17)$$

where  $W_{O,nn}^{\text{cov}}$  the observability covariance matrix of the system,  $W_{O,pp}^{\text{cov}}$  the covariance of the outputs caused by changes in the parameters, and  $W_{O,np}^{\text{cov}}$  and  $W_{O,pn}^{\text{cov}}$  the covariance of the outputs resulting from changes in the states and parameters. The optimal sensor location for parameter estimation is computed by maximizing the traces of  $W_{O,pp}^{\text{cov}}$ . The traces of  $W_{O,pp}^{\text{cov}}$  in CASEs 1 and 2 are plotted for possible sensor locations in Figs. 6 and 7. Figs. 6 and 7 are similar to

Figs. 2 (left) and 3 (left), respectively. That is, the trace of  $W_{O,pp}^{\text{cov}}$  is useful as a criterion for judging where the sensors should be located. On the other hand, the trace and determinant of  $W_{O,pp}^{\text{cov}}$  in CASE 3 are plotted in Figs. 8 and 9, respectively. As compared with Fig. 4, it is clarified that the determinant of  $W_{O,pp}^{\text{cov}}$  is effective as a criterion of optimal sensor locations for estimating multi-parameters.

## 5. OPERATION POLICY FOR MCPs

The production capacity of MCPs is usually increased by numbering-up, which means the repetition of a microdevice. One of the critical operational issues of MCPs with numbering-up structure is to keep a uniform flow distribution among parallelized microdevices even when blockage occurs in one or more microdevice. Since it is not practical to install flow controllers in all the microdevices, a simple and effective operation policy against blockage occurrence needs to be developed. In this work, two types of operation policies, total flow control and pressure drop control, are compared from the viewpoint of flow uniformity when blockage occurs.

### 5.1 Total Flow Control and Pressure Drop Control

To maintain the desired product quality, it is important to keep a uniform flow rate in each microdevice of the micro chemical plant when blockage occurs, because flow maldistribution worsens the performance of the micro chemical plant. In this research, pressure drop control is proposed to achieve the uniform flow distribution.

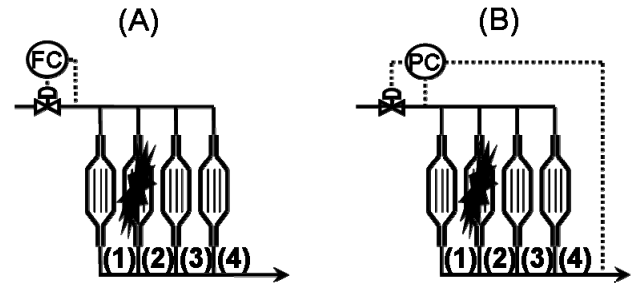


Fig. 10. Parallelized microdevices under two operation policies: (A) total flow control and (B) pressure drop control.

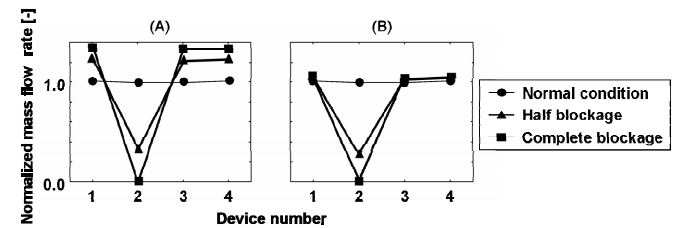


Fig. 11. Mass flow rate of each microdevice under blockage occurrence: (A) total flow control and (B) pressure drop control.

A micro chemical plant consisting of four parallelized microdevices in Fig. 10 is used to demonstrate the difference of two operation policies, total flow control and pressure drop control. When blockage occurs in microdevice 2, the flow distribution under the pressure drop control is derived by simulation and compared with that under the total flow control. In Fig. 10, reactant is fed to the parallelized microdevices at 0.1 m/s in the normal condition. The physical properties of the reactant are assumed to be the same as water (293 K). The results are shown in Fig. 11. In the case of blockage occurrence, mass flow rates of unblocked microdevices are significantly increased under the total flow control (Fig. 11 left), while they are kept constant at the value in a normal condition under pressure drop control (Fig. 11 right). These results show that the proposed pressure drop control is effective in making flow distribution uniform even when blockage occurs.

## 5.2 Comparison of Control Structures in Pressure Drop Control

In the previous section, it was confirmed that pressure drop control is superior to total flow control in realizing uniform flow distribution among unblocked microdevices when blockage occurs. In this section, two different control structures based on pressure drop control, pumping pressure control and pressure drop control over the parallelized section, are investigated.

### 5.2.1 Experimental Apparatus

Micro chemical plants having four or eight parallelized microdevices are used to grasp the distinction between two control structures. A schematic drawing of a micro chemical plant having four parallelized microdevices is shown in Fig. 12. Reactant is fed with a double plunger pump. The product line is open to the atmosphere. The flow rate of each microdevice is measured by using an in-line mass flow meter, and blockage in each microdevice is artificially realized by closing the valve located between the pump and each microdevice. Each microdevice consists of an SUS tube having 0.3 mm inner diameter and 2 m in length. In addition, an SUS tube with 0.5 mm in inner diameter and various lengths is installed after the parallelized microdevices to represent units that are not necessary to be parallelized. Hereafter, this section is referred to as a residence time section. The pressure drops over the parallelized section and

the residence time section are denoted by  $\Delta Pa$  and  $\Delta Pb$ , respectively. The ratio of  $\Delta Pa$  to  $\Delta Pb$  is changed by adjusting the length of the residence time section.

### 5.2.2 Pumping Pressure Control

Under pumping pressure control, the double plunger pump is operated at constant pumping pressure. In experiments, pumping pressure is kept at a gauge pressure of 500 kPa – 1 MPa. Pressure drop over the whole micro chemical plant is kept constant under pumping pressure control, because the product line is open to the atmosphere.

The influence of blockage on flow distribution under pumping pressure control is investigated through both simulations and experiments with changing the ratio  $\Delta Pa/\Delta Pb$  in the range of one-fifth to seven. The first step in the experimental procedure is to adjust the pumping pressure to realize a total flow rate of 12 mL/min. This operating condition is regarded as the normal condition. Then, microdevice 1 is artificially blocked by closing the valve. In 300 s, the micro chemical plant is returned to the normal condition by opening the valve. These procedures are repeated for the other valves to imitate blockage in the other microdevices.

Figure 13 shows the normalized average mass flow rate, which is defined as the ratio of average mass flow rate of unblocked microdevices under blockage occurrence to that under the normal condition at each  $\Delta Pa/\Delta Pb$ . There is little difference between the results of experiments and those of CFD simulations. The normalized average mass flow rate becomes closer to the flow rate under the normal condition as  $\Delta Pa/\Delta Pb$  becomes larger. In other words,  $\Delta Pa$  should be significantly larger than  $\Delta Pb$  to keep the flowrate of unblocked microdevices unchanged when blockage occurs. It is concluded that pumping pressure control is effective to realize uniform flow distribution when the pressure drop over the parallelized section is dominant.

### 5.2.3 Pressure Drop Control Over the Parallelized Section

The flow uniformity achieved by pumping pressure control depends on  $\Delta Pa/\Delta Pb$ , which is the ratio of the pressure drop over the parallelized section to that over the residence time section. The flow uniformity in the parallelized microdevices deteriorates when  $\Delta Pa/\Delta Pb$  is small. In this subsection,

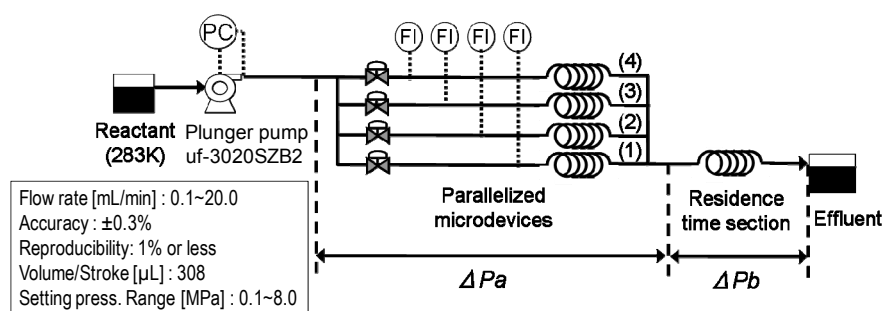


Fig. 12. Micro chemical plant under pumping pressure control.

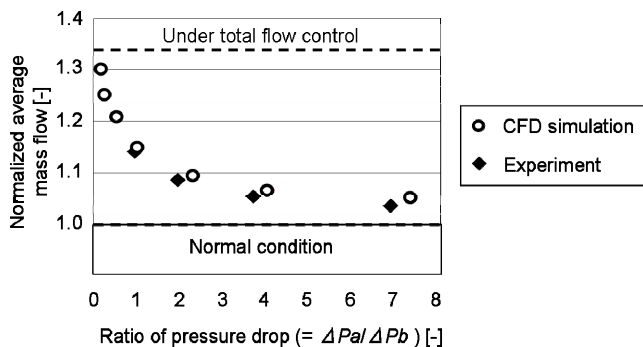


Fig. 13. Influence of blockage on the mass flow rate.

another pressure drop control structure where  $\Delta Pa$  is directly controlled by manipulating the flow rate of the bypass line is proposed.

The performance of the proposed control structure is evaluated experimentally by using the micro chemical plants with four (Type A) and eight (Type B) parallelized microdevices. The plunger pump is operated so that the total flow rate is kept constant. The other conditions are the same as those in the previous subsection.

The experimental results for a Type A plant are shown in Fig. 14. The top and bottom figures correspond to the case where  $\Delta Pa/\Delta Pb = 50$  and  $\Delta Pa/\Delta Pb = 1$ , respectively. In the range of 0–300 s, the micro chemical plant is operated under the normal condition. The difference in flow rate between microdevices 1 and 2 is due to the degree of precision in the fabrication. When blockage occurs in microdevice 1 at 300 s, the flow rate of microdevice 1 goes to zero instantaneously and the flow rate of microdevice 2 deviates from its set-point. However, the flow rate of microdevice 2 returns to the normal level in a few tens of seconds. Flow rate deviation becomes small when blockage occurs gradually. The transient responses of microdevices 3 and 4 are similar to that of microdevice 2; they are not shown in Fig. 14 to identify the transient response of each microdevice easier. The top and bottom figures in Fig. 14 show almost the same profiles. This result shows that the efficiency of the proposed control structure does not depend on  $\Delta Pa/\Delta Pb$ .

The experimental result of a Type B plant is almost the same as that of the Type A plant. These results show that the proposed control structure has the function of keeping the flow rate of the unblocked devices constant regardless of the changes in  $\Delta Pa/\Delta Pb$  and the number of parallelized microdevices.

## 6. CONCLUSIONS

In this study, sensor locations for effective fault diagnosis of TMR are investigated. It is clarified that two different faults are accurately diagnosed by using only two wall temperature sensors, which are optimally located in the axial direction of TMR. In addition, the optimality criteria for sensor locations in TMRs are investigated. The results obtained from case studies demonstrate that the criteria based on observability covariance matrix are effective and their maximization allows

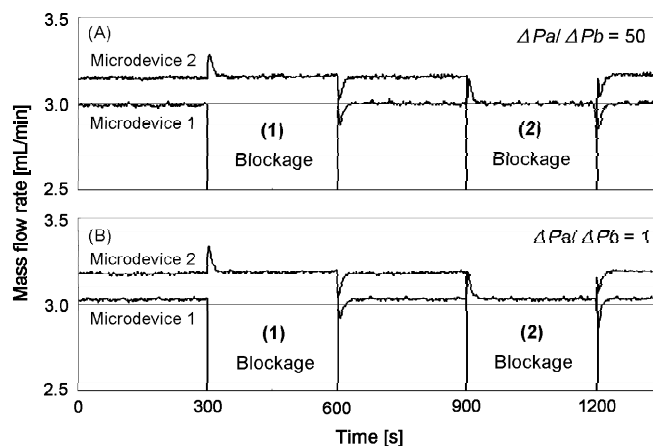


Fig. 14. The time series of mass flow rate in each microdevice in Type A: (A)  $\Delta Pa/\Delta Pb = 50$ , (B)  $\Delta Pa/\Delta Pb = 1$ .

one to determine where the sensors should be located. Finally, we have discussed operation policies and control structures for micro chemical plants with an external numbering-up structure. Two operation policies, total flow control and pressure drop control, were compared. The simulation result shows that the pressure drop control is effective to keep a uniform flow distribution among the parallelized microdevices even when blockage occurs. In addition, two control structures based on pressure drop control, pumping pressure control and pressure drop control over the parallelized section, were investigated experimentally. The former control structure is simple. However, this structure functions only when the ratio of the pressure drop over the parallelized section to that over the residence time section,  $\Delta Pa/\Delta Pb$ , is large. On the other hand, the latter control structure can make the flow distribution uniform for any  $\Delta Pa/\Delta Pb$ .

## REFERENCES

- Dochain, D., Tali-Maamar, N., and Babary, J. P. (1997). On Modeling, Monitoring and Control of Fixed Bed Bioreactors, *Comp. Chem. Eng.*, 21 (11), 1255-1266.
- Hessel, V., Hardt, S., and Lowe, H. (2005). Chemical Micro Process Engineering: Fundamentals, Modelling and Reactions. *Wiley, VCH, Weinheim*.
- Kano, M., Fujioka, T., Tonomura, O., Hasebe, S., and Noda, M. (2007). Data-based and Model-based Blockage Diagnosis for Stacked Microchemical Processes. *Chem. Eng. Sci.*, 62 (4), 1073-1080.
- Muller, P. C. and Weber, H. I. (1972). Analysis and Optimization of Certain Qualities of Controllability and Observability for Linear Dynamical Systems, *Automatica*, 8, 237-246.
- Singh, A. K. and Hahn, J. (2005). Determining Optimal Sensor Locations for State and Parameter Estimation for Stable Nonlinear Systems, *Ind. Eng. Chem. Res.*, 44, 5645-5659.
- van den Berg, F. W. J., Hoefsloot, H. C. J., Boelens, H. F. M., and Smilde, A.K. (2000). Selection of Optimal Sensor Position in a Tubular Reactor Using Robust Degree of Observability Criteria, *Chem. Eng. Sci.*, 55, 827-837.